NANO LETTERS

Letter

pubs.acs.org/NanoLett

Highly Narrowband Photomultiplication Type Organic Photodetectors

Wenbin Wang,[†] Fujun Zhang,*[,†] Mingde Du,[‡] Lingliang Li,[†,§] Miao Zhang,[†] Kai Wang,[†] Yongsheng Wang,[†] Bin Hu,[†,∥] Ying Fang,*[,‡] and Jinsong Huang*[,§]

[†]Key Laboratory of Luminescence and Optical Information, Ministry of Education, Beijing Jiaotong University, Beijing 100044, People's Republic of China

[‡]National Center for Nanoscience and Technology, Beijing 100190, People's Republic of China

[§]Department of Mechanical and Materials Engineering and Nebraska Center for Materials and Nanoscience, University of Nebraska-Lincoln, Lincoln, Nebraska 68588-0656, United States

[∥]Department of Materials Science and Engineering, University of Tennessee, Knoxville, Tennessee 37996, United States

S *Supporting Information*

ABSTRACT: Filterless narrowband response organic photodetectors (OPDs) present a great challenge due to the broad absorption range of organic semiconducting materials. The reported narrowband response OPDs also suffer from low external quantum efficiency (EQE) in the desired response window and low rejection ratio. Here, we report highly narrowband photomultiplication (PM) type OPDs based on P3HT:$PC_{71}BM$ (100:1, wt/wt) as active layer without an optical filter. The full width at half-maximum (fwhm) of the PM-type OPDs can be well retained less than 30 nm under different biases. Meanwhile, the champion EQE and rejection ratio approach 53 500% and 2020 at −60 V bias, respectively. The small fwhm should be attributed to the sharp absorption edge of active layer with small amount of $PC_{71}BM$. The PM phenomenon is attributed to hole tunneling injection from the external circuit assisted by trapped electron in $PC_{71}BM$ near the Al electrode under light illumination. These highly narrowband PM-type OPDs should have great potential applications in sensitively detecting specific wavelength light and be blind to light outside of the desired response window.

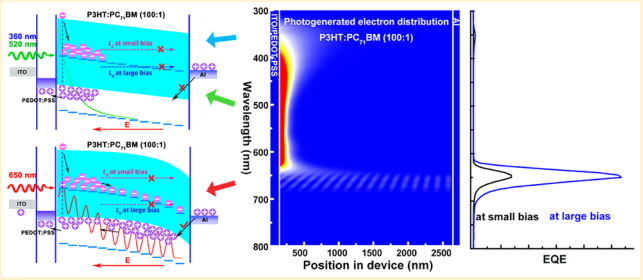

KEYWORDS: *Organic photodetectors, photomultiplication, narrowband response, photogenerated electron distribution, absorption edge*

Organic photodetectors (OPDs) with narrowband response present a great challenge due to the broad absorption range of organic semiconducting materials. Narrowband response OPDs are widely demanded for applications where specific wavelength light is needed to be detected, such as surveillance, fluorescence microscopy, and defense applications.[1−6] In fact, an excellent performance narrowband response OPD should have the following characteristics: (i) narrow full width at half-maximum (fwhm) of the desired response window; (ii) high external quantum efficiency (EQE) in the desired response window and be blind to light outside of the desired response window, that is, a high rejection ratio; and (iii) low dark current density (J_D) in combination with large linear dynamic range (LDR).[7,8] Narrowband response OPDs can be obtained by combining broadband OPDs with bandpass optical filters to select the desired response window or by using organic semicoducting materials with narrow absorption range to prepare the active layers. However, the former approach inevitably decreases the responsivity of OPDs due to the optical transmission delays, attenuations, and complicated designs.[9,10] Despite these issues, optical filters can hardly cover all the desired response windows. For the latter approach, narrowband OPDs with ultraviolet (UV) light response can be obtained by using wide bandgap materials to prepare the active layers.[11,12] However, this method is invalid in obtaining high-performance narrowband response visible and near-infrared (NIR) light OPDs. Meredith et al. proposed a new strategy to manipulate internal quantum efficiency of photodetectors via the charge collection narrowing (CCN) concept, that is, light with different wavelength has different charge collection efficiency because of their different penetration depth, and narrowband red or NIR OPDs were successfully fabricated.[13] Recently, narrowband response solution-processed perovskite photodetectors with tunable spectral response range have been achieved by using the CCN strategy.[14] Highly narrowband with fwhm of EQE spectra below 20 nm was achieved using

Received: December 31, 2016
Revised: January 27, 2017
Published: February 6, 2017

DOI: 10.1021/acs.nanolett.6b05418
Nano Lett. 2017, 17, 1995−2002

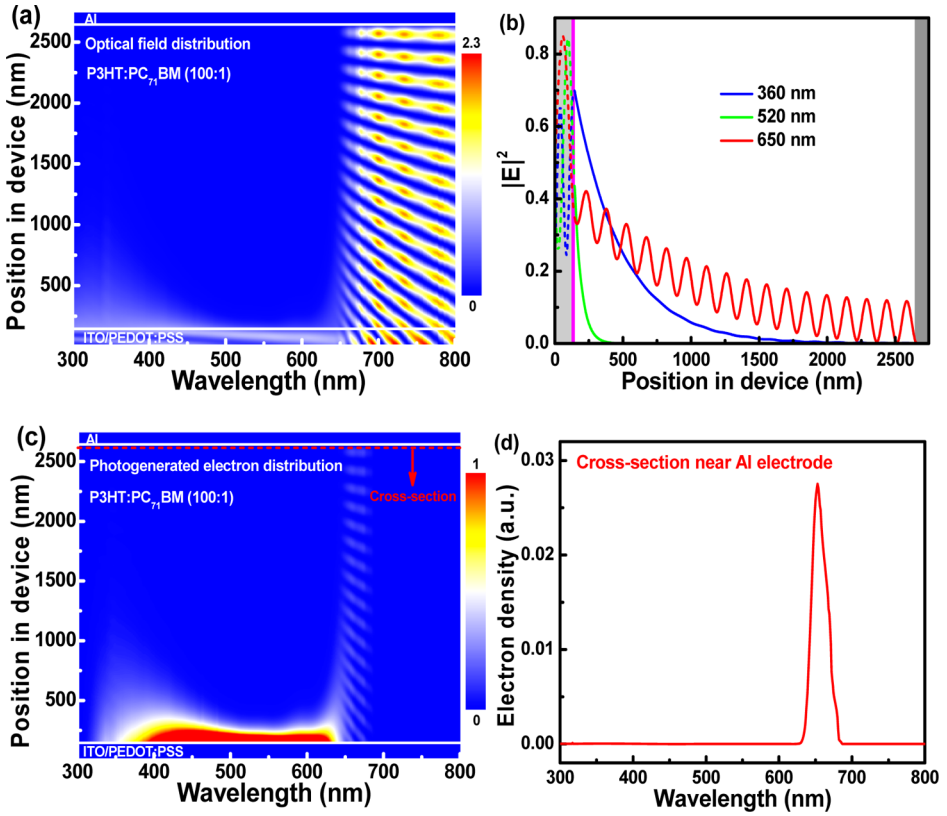

Figure 1. (a) Simulated optical field distribution in OPDs with 2.5 μm thick P3HT:$PC_{71}BM$ (100:1, wt/wt) active layer. (b) Optical field intensities in the active layer for three typical wavelengths, 390, 520, and 650 nm; (c) Normalized photogenerated electron distribution in P3HT:$PC_{71}BM$ (100:1, wt/wt) active layer. (d) Photogenerated electron distribution on the cross-section that is located approximately 50 nm away from Al electrode.

perovskite single crystals by quenching the short-wavelength light induced carriers at the surface of the crystals, which presents a different strategy for narrowband response.[15] However, the champion EQE of the reported narrowband response photodetectors without a gain was relatively low (<30%), because most photogenerated charge carriers in the desired response window cannot be efficiently collected by individual electrode. Meanwhile, the narrowband detection capability will be lost at large biases (>1 V) due to the improved charge carriers collection.

Photomultiplication (PM) phenomenon has been realized based on organic semiconducting materials to obtain highly sensitive OPDs,[16−21] which inspires us to develop narrowband response PM-type OPDs. The interfacial charge trap-induced secondary charge injection has been developed by doping CdTe or PbS quantum dots (QDs) to introduce a gain in narrowband response organic and hybrid photodetectors, and the narrowest fwhm of 50 nm was achieved.[7,22] An initial combination of high gain mechanism with narrowband response demonstrated the enhanced sensitivity to the narrowband response photodetectors. Despite the gain introduced by doping QDs, the fwhm of the narrowband response photodetectors may also limited by the absorption of the introduced QDs in the long-wavelength range. Recently, we reported PM-type OPDs with a small amount of $PC_{71}BM$ in the active layer as electron traps due to the large difference between the lowest unoccupied molecular orbitals (LUMOs) of $PC_{71}BM$ and P3HT.[23] The trapped electrons in $PC_{71}BM$ near the Al electrode work as space charges to induce interfacial band bending, leading to efficient hole tunneling injection from the external circuit under light illumination.[24] The OPDs with thin active layers exhibited a broad spectral response range from 350 to 650 nm because eletrons generated by different wavelengths of light can be trapped in $PC_{71}BM$ near the Al electrode to induce hole tunneling injection from the external circuit. In this article, highly narrowband PM-type OPDs with fwhm less than 30 nm were successfully fabricated by applying thick P3HT:$PC_{71}BM$ (100:1, wt/wt) active layer to adjust the photogenerated electron distribution near the Al electrode. The champion EQE value and rejection ratio of the OPDs remarkably increased to 53 500% and 2020 along with the bias increases to −60 V, respectively. Meanwhile, the spectral response range of the PM-type OPDs can be well-retained with fwhms less than 30 nm even at large biases.

Results and Discussion. The optical field distributions in the OPDs consisting of ITO (120 nm)/PEDOT:PSS (25 nm)/P3HT:$PC_{71}BM$ (100:1, wt/wt) (0.3, 1, 2, 2.5 μm)/Al (100 nm) were simulated based on the transfer matrix method.[25] The optical constants (refractive index n and extinction coefficient k) of P3HT:$PC_{71}BM$ (100:1, wt/wt) blend film used in the simulations are shown in Figure S1. The simulated optical field distributions in OPDs with different active layer thicknesses are shown in Figure S2. On the basis of the optical field distributions dependence on active layer thickness, incident light with wavelengths shorter than 630 nm can be completely absorbed when the active layer thickness increases to approximately 2.5 μm, as shown in Figure 1a. The fringes that originate from the interference between incident light and reflected light from the Al electrode gradually become apparent when incident light wavelengths exceed 650 nm. To investigate

DOI: 10.1021/acs.nanolett.6b05418
Nano Lett. 2017, 17, 1995−2002

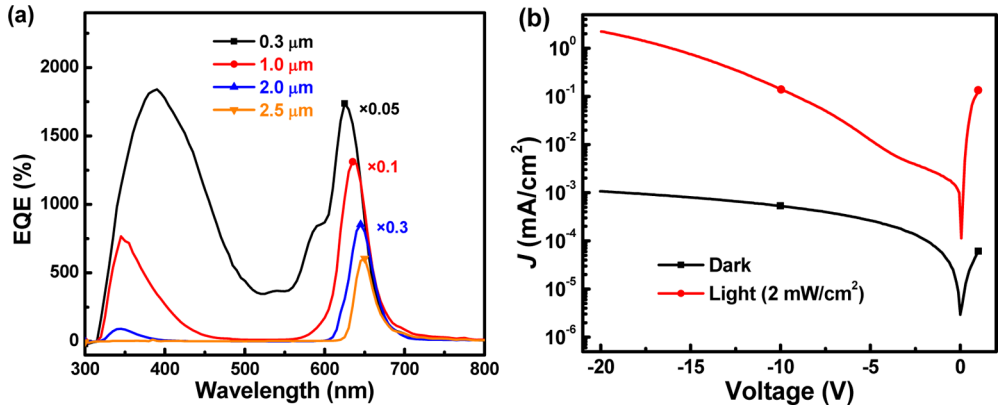

Figure 2. (a) EQE spectra of OPDs with different active layer thicknesses. (b) $J-V$ curves of the OPDs with 2.5 μm thick active layer in dark and under white light illumination with an intensity of 2 mW/cm^2.

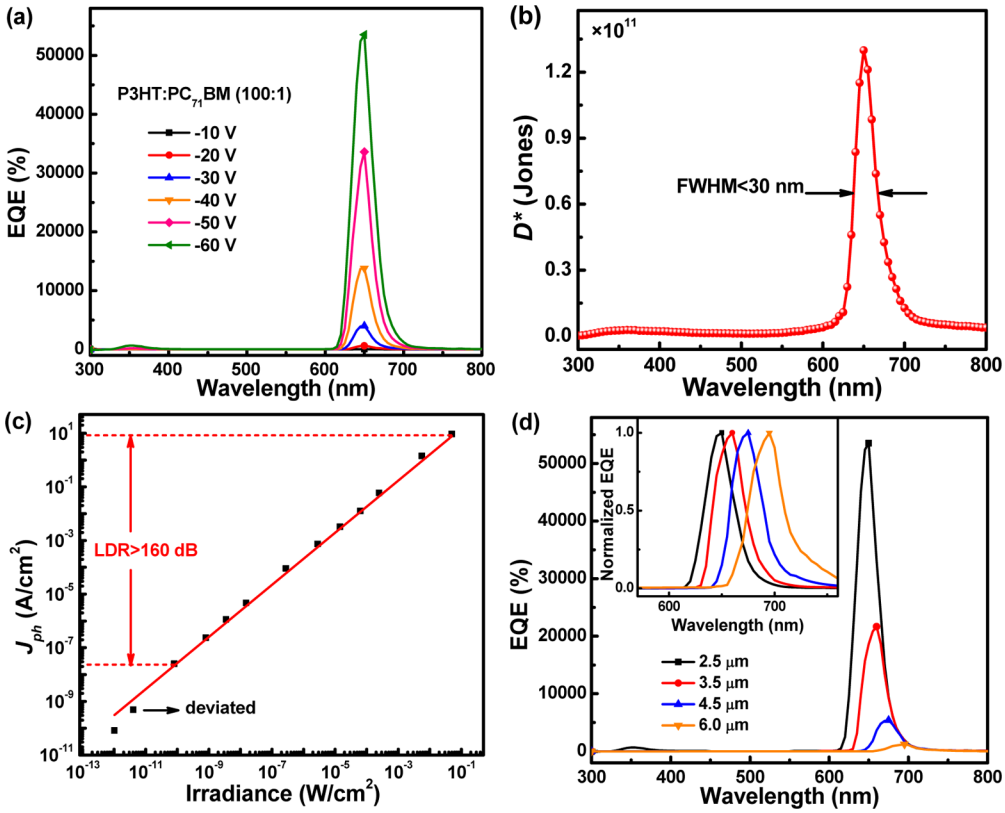

Figure 3. (a) EQE spectra of the optimized highly narrowband PM-type OPDs at different biases. (b) Specific detectivity (D^*) dependence on incident light wavelength of the optimized highly narrowband PM-type OPDs at −10 V bias. (c) The LDR of the optimized OPDs measured at −60 V bias, the solid red line is the linear fitting. (d) EQE spectra of the high narrowband PM-type OPDs dependence on active layer thickness under electric field intensity of 2.4 × 10^7 V/m; the inset is the normalized EQE spectra.

light transmission of different wavelengths in the active layer, the optical field distributions of three typical wavelengths (360, 520, and 650 nm) are shown in Figure 1b. The optical field intensities ($|E|^2$) of 360 and 520 nm light rapidly decay to zero along with the light transmission in the active layer, which obeys Beer−Lambert law.[22,26] For 650 nm light, a periodic oscillation is clearly observed due to the interference phenomenon. The photogenerated electron distribution can be calculated in the active layer according to the optical field distribution, as shown in Figure 1c. Obviously, most of photogenerated electrons are produced at the vicinity of ITO electrode under short-wavelength light illumination, especially in the strong absorption range of the active layer. These photogenerated electrons are difficult to be transported toward the Al electrode under reverse bias due to the lack of electron percolation channels in the P3HT:PC$_{71}$BM active layer with only 1 wt % of PC$_{71}$BM. Therefore, the OPDs almost had no response under short-wavelength light illumination. To intuitively investigate photogenerated electron distributions in PC$_{71}$BM near the Al electrode, a cross-section was chosen that is approximately 50 nm away from the Al electrode, as marked by the red dotted line in Figure 1c. The photogenerated electron distribution on this cross-section is shown in Figure 1d. A narrow distribution of photogenerated electrons is

DOI: 10.1021/acs.nanolett.6b05418
Nano Lett. 2017, 17, 1995−2002

obtained with a fwhm of approximately 30 nm. According to the working principle of the PM-type OPDs, only the trapped electrons near the Al electrode can induce interfacial band bending for efficient hole tunneling injection from the external circuit. Therefore, narrowband response PM-type OPDs may be realized on the basis of the above theoretical simulation and analysis.

A series of OPDs were fabricated with different thicknesses of P3HT:$PC_{71}BM$ (100:1, wt/wt) as active layers. The pristine blend films were directly annealed at 100 °C for 1 min to obtain uniform distribution of $PC_{71}BM$ in the thick active layers during the drying process. The X-ray photoelectron spectroscopy (XPS) was used to investigate the composition variation at the top surface of active layers with or without annealing treatment, as shown in Figure S3. The XPS data indicate that the C (1s)/S (2p) atomic ratio at the top surface of the active layer with annealing treatment is similar to the theoretical C (1s)/S (2p) atomic ratio of P3HT:$PC_{71}BM$ (100:1, wt/wt) blend film, and the detailed discussions are shown in the Supporting Information. The EQE spectra of all OPDs with different thicknesses of active layer were measured at −20 V bias and are shown in Figure 2a. Light intensity spectrum of the used monochromatic light is shown in Figure S4. It is apparent that the EQE values decreased along with the increase of active layer thickness, especially for light with wavelengths shorter than 600 nm. When the active layer thickness increased to approximately 2.5 μm, the OPDs exhibited a highly narrowband with a fwhm of 27 nm, and the PM phenomenon was still preserved (EQE of approximately 600%). The current density versus voltage ($J-V$) curves of OPDs consisting of 2.5 μm thick active layer were measured in dark and under white light illumination with an intensity of 2 mW/cm^2, as shown in Figure 2b. In dark conditions, electrons can hardly be injected from ITO onto the LUMO level of $PC_{71}BM$ due to their limited contact interface. Meanwhile, electrons can hardly be transported in the active layer due to the lack of percolation channels. To verify charge carriers transport ability in the active layer, electron-only devices with a structure of ITO/Al/LiF/P3HT:$PC_{71}BM$(100:1, wt/wt)/LiF/Al and hole-only devices with a structure of ITO/PEDOT:PSS/P3HT:$PC_{71}BM$ (100:1, wt/wt)/MoO_3/Ag were fabricated, the $J-V$ curves of devices were measured and are shown in Figure S5. It is apparent that current density of electron-only devices was about 5 orders of magnitude smaller than that of the hole-only devices at the same bias, which further confirms the limited electron transport in the active layer. It should be highlighted that holes can hardly be injected from Al onto the highest occupied molecular orbital (HOMO) level of P3HT due to the large injection barrier of 0.9 eV, resulting in a rather low dark current. Under light illumination, holes can be easily injected from Al electrode due to the interfacial band bending induced by trapped electrons in $PC_{71}BM$ near the Al electrode, which can be confirmed from the exponential increased light current density (J_L) along with the increase of bias. The J_L is 3 orders of magnitude larger than the J_D at −20 V bias, indicating that the OPDs have a significant photoresponse feature. This phenomenon means that trapped electrons in $PC_{71}BM$ near the Al electrode act like a key that triggers hole tunneling injection from the external circuit under light illumination.[24] Once holes are injected from the external circuit, the holes can be efficiently transported along the channels formed by P3HT under reverse bias, resulting in the markedly increased J_L or sensitive photoresponse of the OPDs.

Figure 3a shows EQE spectra of the PM-type OPDs with 2.5 μm thick active layer at different biases. It is apparent that EQE values dramatically increased along with bias, and the highest EQE approached 53 500% at −60 V bias, corresponding to a responsivity (R) of 278 A/W. The enhanced EQE along with the increase of bias may be attributed to the enhanced hole tunneling injection and the improved hole transport in active layer at larger biases. Meanwhile, the rejection ratio, defined as the EQE ratio of 650 to 520 nm, was dramatically increased from 90 to 2020 when the bias increased from −10 to −60 V. To clearly exhibit the detailed performance of the optimized highly narrowband PM-type OPDs, the key parameters of the OPDs under different biases are summarized in Table 1. Most importantly, the fwhms of EQE spectra of the optimized highly narrowband PM-type OPDs can be well retained at less than 30 nm even at large biases. This means that the photogenerated electron distribution in $PC_{71}BM$ near the Al electrode can be kept constant along with the increase of bias. The photogenerated electrons can hardly be transported along the dispersed $PC_{71}BM$ in the thick active layer, leading to the unchanged number of trapped electrons in $PC_{71}BM$ near the Al electrode. Therefore, the high narrowband can be well retained at large biases, which is beneficial to improve the rejection ratio for the PM-type OPDs working at large biases. It is worth noting that the narrowband response OPDs also exhibit good stability even after 15 cycles of EQE spectra measurement at −60 V bias, as shown in Figure S7.

Table 1. Detailed EQE Values, Rejection Ratios, and fwhms of the Optimized Highly Narrowband PM-Type OPDs under Different Biases

bias	EQE (%)[a]	rejection ratio[b]	fwhm (nm)
−10 V	49	90	29
−20 V	600	370	27
−30 V	4,000	830	26
−40 V	13,800	1,340	27
−50 V	33,600	1,750	28
−60 V	53,500	2,020	28

[a]EQE: EQE values at 650 nm. [b]Rejection ratio: the EQE ratio of 650−520 nm.

The narrowband response PM-type OPDs have dark current as low as 19.4 nA at −10 V bias due to the limited charge carriers injection and limited electron transport, resulting in the rather small shot noise. To investigate the other possible noise contributions, such as $1/f$ noise (also called flicker noise) and thermal noise, the noise current (I_{noise}) was directly measured from the Fourier transform of the dark current versus time at −10 V bias, as shown in Figure S8. It is obvious that the measured noise current in the OPDs was dominated by $1/f$ noise at low frequencies (f < 10 Hz) and is barely sensitive to the frequency at high frequencies (f > 10 Hz). The noise equivalent power (NEP) and specific detectivity (D^*) can be calculated according to the following equations

$$\mathrm{NEP} = \frac{I_{noise}}{R} \quad (1)$$

$$D^* = \frac{\sqrt{A}}{\mathrm{NEP}} \quad (2)$$

where A is the active area of the device (here is 3.8 mm^2 in this study) and R is 0.255 A/W under 650 nm light illumination at

DOI: 10.1021/acs.nanolett.6b05418
Nano Lett. 2017, 17, 1995−2002

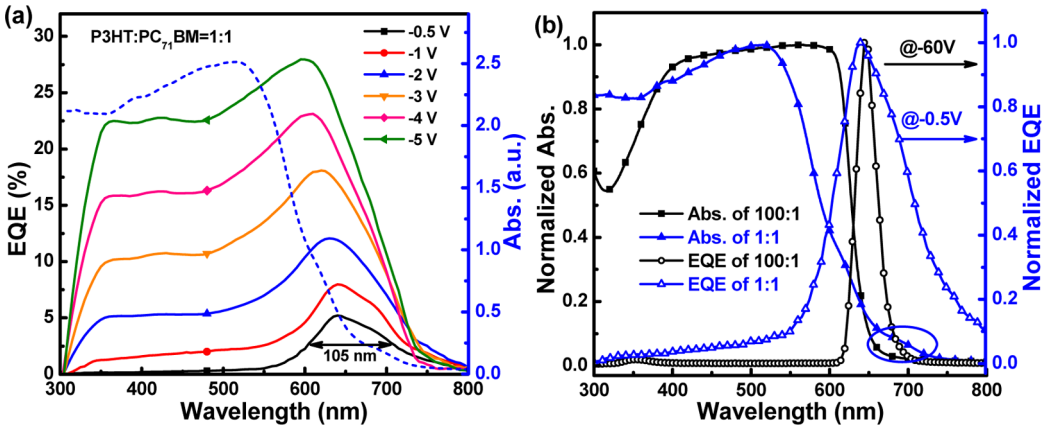

Figure 4. (a) EQE spectra of the OPDs with P3HT:$PC_{71}BM$ (1:1, wt/wt) as the active layer at different reverse biases. (b) Normalized EQE spectra of the PD and PM-type OPDs as well as corresponding absorption spectra of the blend films.

−10 V bias. As shown in Figure S9, the lowest NEP of the narrowband response OPDs is approximate 1.5×10^{-12} W/$Hz^{1/2}$ at a low frequency of 1 Hz at 650 nm, which means the lowest detectable light intensity at a signal-to-noise ratio of unity is 39.5 pW/cm^2 at −10 V bias. On the basis of the NEP, the D^* dependence on incident light wavelength of the narrowband response OPDs was calculated, as shown in Figure 3b. The highest D^* is approximately 1.3×10^{11} cm $Hz^{1/2}$/W (Jones) under 650 nm light illumination at −10 V bias, which is comparable with the reported narrowband response PM-type OPDs.[7,22] The linear dynamic range (LDR) is a crucial parameter for image sensors, because photodetectors need to operate in a broad light intensity range. The LDR of the OPDs was measured by recording the steady-state photocurrent under 650 nm light illumination with different light intensities from 1.02 pW/cm^2 up to 0.05 W/cm^2, as shown in Figure 3c. The photocurrent of the OPDs exhibits a linear response with light intensity increases from 80.4 pW/cm^2 to 0.05 W/cm^2. A linear response of approximately 8 orders of magnitude corresponds to a LDR of 160 dB.[2,27,28] Such a large LDR indicates that the PM-type OPDs have the functionality to detect light with a large range of light intensity. The PM-type OPDs began to lost their linearity when incident light intensity is lower than 80.4 pW/cm^2, which can be explained by the weaken hole tunneling injection resulting from the rather less trapped electrons in $PC_{71}BM$ near the Al electrode. The transient photocurrent of the OPDs was measured under 650 nm light illumination at −60 V bias, as shown in Figure S10. The transient photocurrent shows a relatively long rise time (J_{ph} increases from 10% to 90% of the saturated J_{ph}) of 0.74 s and a short fall time (J_{ph} decreases from 90% to 10% of the saturated J_{ph}) of 0.43 s. The number of trapped electrons in $PC_{71}BM$ near the Al electrode needs to reach a dynamic balance between electron trapping and recombination with holes after the excitation light is switched on, resulting in a relatively long rise time of transient photocurrent. The trapped electrons in $PC_{71}BM$ near the Al electrode will be recombined with holes when the excitation light is switched off, leading to a relatively short fall time of transient photocurrent.

It is known that the active layer thickness has a great effect on optical field and photogenerated electron distributions, especially near the Al electrode. The EQE spectra of OPDs with different active layer thicknesses were measured under the same electric field of 2.4×10^7 V/m, as shown in Figure 3d. It is apparent that the EQE values were markedly decreased with the increase of active layer thickness under the same electric field, which may be mainly attributed to the decreased number of trapped electrons in $PC_{71}BM$ near the Al electrode in the thick active layers. The normalized EQE spectra of all OPDs are shown in the inset of Figure 3d. There is an apparent EQE spectral peak redshift from 650 to 695 nm as the active layer thickness gradually increases up to 6 μm. Along with the increase of active layer thickness, only incident light with longer wavelengths can penetrate the entire active layer because the active layers have weaker absorption in the wavelength range. Therefore, the peak of photogenerated electron distribution near the Al electrode should be shifted to the longer wavelength range along with the increase of active layer thickness, resulting in the red-shifted EQE peak of the corresponding OPDs.

It is thus interesting to investigate the effect of $PC_{71}BM$ doping ratios on the performance of the narrowband response OPDs. The OPDs were fabricated with 2.5 μm thick P3HT:$PC_{71}BM$ (1:1, wt/wt) as the active layer. The EQE spectra of the OPDs were measured at different biases and are shown in Figure 4a. All the corresponding EQEs are much lower than 100% in the whole spectral range, indicating that the OPDs work as a PD model. When the bias is −0.5 V, the OPDs exhibit narrowband response with a fwhm of approximately 105 nm. The narrowband response of this PD-type OPDs could be well explained by the CCN concept proposed by Meredith et al.[13] The maximum EQE of the OPDs is about 5% at −0.5 V bias due to the rather poor photogenerated charge carrier collection. Meanwhile, EQE values and spectral response range of the OPDs can be increased along with the increase of bias. Such phenomenon should be attributed to the enhancement of photogenerated charge carriers transport and collection at large biases. The fwhms of EQE spectra increased from 105 to 355 nm and the rejection ratios (EQE ratio of highest value to that at 520 nm) decreased from 13.4 to 1.2 along with the bias increases, indicating that the PD-type OPDs lost the narrowband detection capability at large biases. According to the photogenerated electron distribution in P3HT:$PC_{71}BM$ (1:1, wt/wt) active layer (shown in Figure S11), most of photogenerated electrons are produced at the vicinity of ITO electrode. These photogenerated electrons can be efficiently transported in the thick P3HT:$PC_{71}BM$ (1:1, wt/wt) active layer and then collected by Al electrode at large biases, resulting in the markedly widened spectral response range. For the PD-type OPDs, the optimized fwhm of EQE spectra is

DOI: 10.1021/acs.nanolett.6b05418
Nano Lett. 2017, 17, 1995−2002

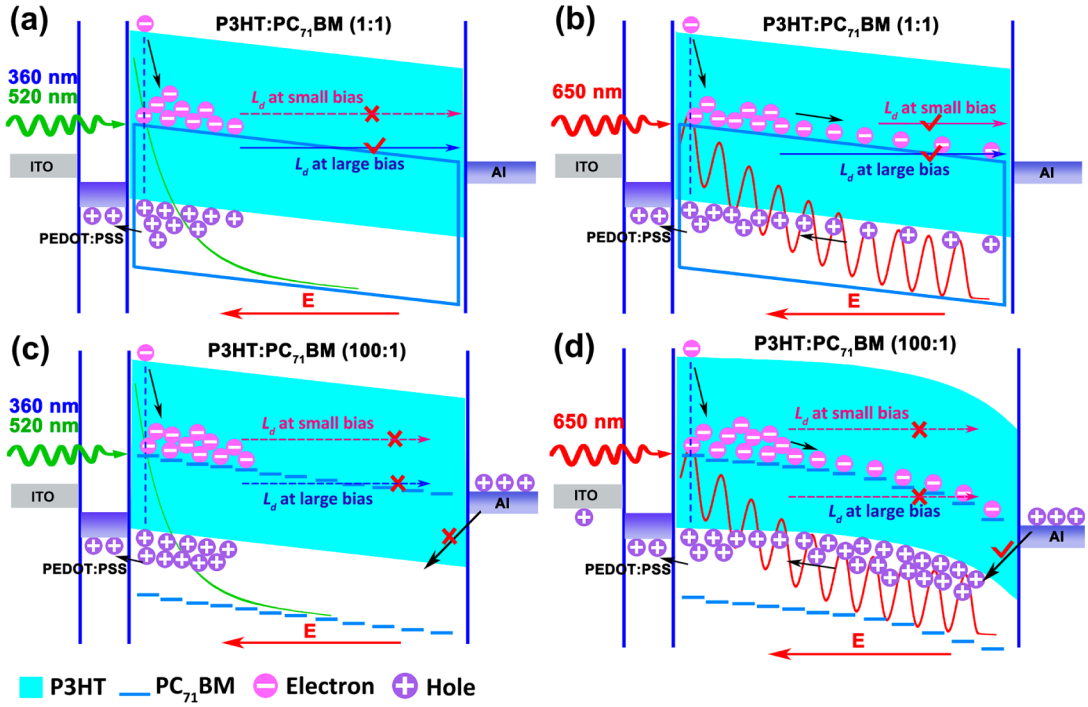

Figure 5. (a) PD-type OPDs under short-wavelength light illumination. (b) PD-type OPDs under 650 nm light illumination. (c) PM-type OPDs under short-wavelength light illumination. (d) PM-type OPDs under 650 nm light illumination.

approximately three times larger than that of the PM-type OPDs. The only difference between the PD-type and PM-type OPDs is the $PC_{71}BM$ doping ratio in active layers. The normalized absorption spectra of the blend films and EQE spectra of the corresponding OPDs are shown in Figure 4b. It is obvious that the thick P3HT:$PC_{71}BM$ (100:1, wt/wt) blend film exhibits a sharp absorption edge in the long-wavelength range. According to the photogenerated electron distribution in the P3HT:$PC_{71}BM$ (100:1, wt/wt) active layer, the narrow photogenerated electron distribution near the Al electrode matches well with the sharp absorption edge of the blend film. On the basis of the working principle of the PM-type OPDs, only the trapped electrons in $PC_{71}BM$ near the Al electrode play a key role in determining hole tunneling injection from the external circuit under light illumination. Therefore, the high narrowband can be well understood according to the sharp absorption edge of P3HT:$PC_{71}BM$ (100:1, wt/wt) blend film. The PD-type OPDs exhibit relatively broad spectral response range with a fwhm of 105 nm even at small bias of −0.5 V. The large fwhm can be attributed to the broad photogenerated electron distribution in the entire active layer under long-wavelength light illumination (shown in Figure S11), which results from the smooth absorption edge of P3HT:$PC_{71}BM$ (1:1, wt/wt) blend film. The corresponding optical constants of P3HT:$PC_{71}BM$ (1:1, wt/wt) blend film and optical field distribution in OPDs with 2.5 μm thick P3HT:$PC_{71}BM$ (1:1, wt/wt) as an active layer are shown in Figure S12. The photoresponse in wavelengths longer than 700 nm should be due to the contribution of $PC_{71}BM$ on photon harvesting, which can be identified from the absorption spectra of blend films with different $PC_{71}BM$ doping ratios, as marked in Figure 4b. The collection of photogenerated charge carriers can be efficiently enhanced along with the bias increases, resulting in the widened spectral response range from 350 to 750 nm. To further clarify the key role of $PC_{71}BM$ in determining the performance of OPDs, the $J-V$ curves of the OPDs with pure P3HT as active layers were measured in the dark and under light illumination, as shown in Figure S13. The OPDs with neat P3HT as active layers exhibit almost no light response, indicating that rather small amounts of $PC_{71}BM$ as electron traps play the critical role in obtaining narrowband response PM-type OPDs.

To fully understand the working principle of the PM and PD-type OPDs, schematic images were drawn to describe the distribution and transport of electrons generated by different wavelengths light in the thick P3HT:$PC_{71}BM$ (1:1 and 100:1, wt/wt) active layers, as shown in Figure 5. The photogenerated electrons are produced at the vicinity of the ITO electrode under short-wavelength light illumination. The photogenerated electrons near ITO electrode will be subject to significant recombination loss due to the high photogenerated carriers concentration and limited electron transport in the thick active layers, especially in the P3HT:$PC_{71}BM$ (100:1, wt/wt) active layers. Therefore, there is almost no response in the short-wavelength range at small biases. The electron drift length (L_D) will be prolonged even to Al electrode in P3HT:$PC_{71}BM$ (1:1, wt/wt) active layers at large biases, resulting in the occurrence of spectral response in the short-wavelength range, as shown in Figure 5a. The photogenerated carriers prefer to distribute throughout the active layers under long-wavelength light illumination, especially for 650 nm wavelength light, as shown in Figure 5b. The photogenerated carriers in the thick active layers will be partially collected by individual electrode at small bias, resulting in the low EQE and relatively narrowband response in long-wavelength range. The collection of photogenerated carriers will be improved at large biases, leading to the enhanced EQE and widened spectral response range. However, serious charge carrier recombination cannot be avoided in the thick active layers, resulting in the relatively low EQE (<30%) at large biases. For light with wavelengths below

DOI: 10.1021/acs.nanolett.6b05418
Nano Lett. 2017, 17, 1995−2002

the optical gap of used materials, the photoresponse of the OPDs will vanish due to the absence of photogenerated carriers in the active layers.

For the PM-type OPDs, only the trapped electrons in $PC_{71}BM$ near the Al electrode can induce interfacial band bending, resulting in the efficient hole tunneling injection from the external circuit under light illumination. Under short-wavelength light illumination, the photogenerated electrons near ITO electrode are hardly trapped in $PC_{71}BM$ near the Al electrode due to the lack of electron percolation channels in the P3HT:$PC_{71}BM$ active layer containing 1 wt % of $PC_{71}BM$. The limited number of trapped electrons in $PC_{71}BM$ near the Al electrode cannot induce interfacial band bending for hole tunneling injection from the external circuit (shown in Figure 5c), resulting in no photoresponse in the short-wavelength range even at large biases. Under long-wavelength light illumination, photogenerated electrons prefer to distribute throughout the active layer due to the interference effect, especially for light with wavelength of approximately 650 nm. Therefore, holes can be easily injected from the external circuit induced by trapped electrons in $PC_{71}BM$ near the Al electrode at small biases. More holes can be injected from the external circuit at large biases, resulting in the dramatically increased EQE. Meanwhile, the key parameters R and rejection ratios of the narrowband response PM-type OPDs can be markedly improved at large biases. The most important thing is that the narrowband response with fwhms less than 30 nm can be well retained for the PM-type OPDs at large biases.

Conclusions. In summary, we successfully demonstrated narrowband response PM-type OPDs with fwhm less than 30 nm based on P3HT:$PC_{71}BM$ (100:1, wt/wt) as the active layers. The small fwhm should be attributed to the sharp absorption edge of active layer with small amount of $PC_{71}BM$. The EQE and rejection ratio of the OPDs approach 53 500% and 2020 at −60 V bias, respectively. Most importantly is that the spectral response range of the PM-type OPDs can be well retained with fwhms less than 30 nm at large biases. The number and distribution of trapped electrons in $PC_{71}BM$ near the Al electrode play a critical role in determining the performance of highly narrowband PM-type OPDs. It is worth noting that this approach can be applied to fabricate spectral tunable narrowband response PM-type OPDs by selecting different optical gap organic semiconducting materials as electron donor or acceptor. It is believed that the highly narrowband PM-type OPDs have great potential applications in which a specific wavelength light needs to be sensitively detected.

■ ASSOCIATED CONTENT

Supporting Information

The Supporting Information is available free of charge on the ACS Publications website at DOI: 10.1021/acs.nanolett.6b05418.

Experimental section; optical constants of P3HT:$PC_{71}BM$ (100:1, wt/wt) blend film; optical field distribution of P3HT:$PC_{71}BM$ (100:1, wt/wt) blend film with different thicknesses; XPS data of the pristine blend films with or without annealing treatment; light intensity spectrum of the monochromatic lights through a monochromator; $J-V$ curves of electron-only and hole-only devices; $J-V$ curves of the OPDs measured from 1 to −60 V bias; EQE spectra of the narrowband response PM-type OPDs; noise current of the narrowband response PM-type OPDs; NEP of the highly narrowband PM-type OPDs; transient photocurrent of the narrowband response PM-type OPDs; photogenerated electron distribution in P3HT:$PC_{71}BM$ (1:1, wt/wt) blend film; optical constants of P3HT:$PC_{71}BM$ (1:1, wt/wt) blend film and optical field distribution in OPDs with P3HT:$PC_{71}BM$ (1:1, wt/wt) as active layer; the $J-V$ curves of ITO/PEDOT:PSS/pure P3HT (2.5 μm)/Al device (PDF)

■ AUTHOR INFORMATION

Corresponding Authors

*E-mail: fjzhang@bjtu.edu.cn.
*E-mail: fangy@nanoctr.cn.
*E-mail: jhuang2@unl.edu.

ORCID

Fujun Zhang: 0000-0003-2829-0735
Ying Fang: 0000-0003-2965-7287
Jinsong Huang: 0000-0002-0509-8778

Notes

The authors declare no competing financial interest.

■ ACKNOWLEDGMENTS

This work was supported by National Natural Science Foundation of China (61377029, 61675017), Fundamental Research Funds for the Central Universities (2016YJS149). Huang thanks the support from National Science Foundation under awards ECCS-1608610 and CMMI-1265834. A portion of this work is based on the data obtained at X-ray photoelectron spectroscopy (4B9B), BSRF. The authors gratefully acknowledge the assistance of the beamline scientists at 4B9B, BSRF during the experiments.

■ REFERENCES

(1) Rauch, T.; Boberl, M.; Tedde, S. F.; Furst, J.; Kovalenko, M. V.; Hesser, G. N.; Lemmer, U.; Heiss, W.; Hayden, O. *Nat. Photonics* **2009**, *3*, 332−336.
(2) Liu, C.; Peng, H.; Wang, K.; Wei, C.; Wang, Z.; Gong, X. *Nano Energy* **2016**, *30*, 27−35.
(3) Zhou, L.; Wang, R.; Yao, C.; Li, X. M.; Wang, C. L.; Zhang, X. Y.; Xu, C. J.; Zeng, A. J.; Zhao, D. Y.; Zhang, F. *Nat. Commun.* **2015**, *6*, 6938.
(4) Nishiwaki, S.; Nakamura, T.; Hiramoto, M.; Fujii, T.; Suzuki, M. *Nat. Photonics* **2013**, *7*, 248−254.
(5) Wan, Y.; Zhou, Y. G.; Poudineh, M.; Safaei, T. S.; Mohamadi, R. M.; Sargent, E. H.; Kelley, S. O. *Angew. Chem., Int. Ed.* **2014**, *53*, 13145−13149.
(6) Kelley, S. O.; Mirkin, C. A.; Walt, D. R.; Ismagilov, R. F.; Toner, M.; Sargent, E. H. *Nat. Nanotechnol.* **2014**, *9*, 969−980.
(7) Shen, L.; Zhang, Y.; Bai, Y.; Zheng, X. P.; Wang, Q.; Huang, J. S. *Nanoscale* **2016**, *8*, 12990−12997.
(8) Lee, M. L.; Chi, P.-F.; Sheu, J. K. *Appl. Phys. Lett.* **2009**, *94*, 013512.
(9) Xu, T.; Wu, Y.-K.; Luo, X.; Guo, L. J. *Nat. Commun.* **2010**, *1*, 1−5.
(10) Park, H.; Dan, Y.; Seo, K.; Yu, Y. J.; Duane, P. K.; Wober, M.; Crozier, K. B. *Nano Lett.* **2014**, *14*, 1804−1809.
(11) Jansen-van Vuuren, R. D.; Pivrikas, A.; Pandey, A. K.; Burn, P. L. *J. Mater. Chem. C* **2013**, *1*, 3532−3543.
(12) Su, Z. S.; Li, W. L.; Chu, B.; Li, T. L.; Zhu, J. Z.; Zhang, G.; Yan, F.; Li, X.; Chen, Y. R.; Lee, C. S. *Appl. Phys. Lett.* **2008**, *93*, 103309.
(13) Armin, A.; Jansen-van Vuuren, R. D.; Kopidakis, N.; Burn, P. L.; Meredith, P. *Nat. Commun.* **2015**, *6*, 6343.

DOI: 10.1021/acs.nanolett.6b05418
Nano Lett. 2017, 17, 1995−2002

(14) Lin, Q. Q.; Armin, A.; Burn, P. L.; Meredith, P. *Nat. Photonics* **2015**, *9*, 687−694.
(15) Fang, Y. J.; Dong, Q. F.; Shao, Y. C.; Yuan, Y. B.; Huang, J. S. *Nat. Photonics* **2015**, *9*, 679−686.
(16) Guo, F. W.; Yang, B.; Yuan, Y. B.; Xiao, Z. G.; Dong, Q. F.; Bi, Y.; Huang, J. S. *Nat. Nanotechnol.* **2012**, *7*, 798−802.
(17) Reynaert, J.; Arkhipov, V. I.; Heremans, P.; Poortmans, J. *Adv. Funct. Mater.* **2006**, *16*, 784−790.
(18) Chen, H. Y.; Lo, M. K. F.; Yang, G. W.; Monbouquette, H. G.; Yang, Y. *Nat. Nanotechnol.* **2008**, *3*, 543−547.
(19) Yuan, Y. B.; Huang, J. S. *Adv. Opt. Mater.* **2016**, *4*, 264−270.
(20) Lee, J. W.; Kim, D. Y.; So, F. *Adv. Funct. Mater.* **2015**, *25*, 1233−1238.
(21) Han, Z. H.; Zhang, H.; Tian, Q. S.; Li, L. L.; Zhang, F. J. *Sci. China: Phys., Mech. Astron.* **2015**, *58*, 1−5.
(22) Shen, L.; Fang, Y. J.; Wei, H. T.; Yuan, Y. B.; Huang, J. S. *Adv. Mater.* **2016**, *28*, 2043−2048.
(23) Wang, W. B.; Zhang, F. J.; Li, L. L.; Gao, M. L.; Hu, B. *ACS Appl. Mater. Interfaces* **2015**, *7*, 22660−22668.
(24) Li, L. L.; Zhang, F. J.; Wang, J.; An, Q. S.; Sun, Q. Q.; Wang, W. B.; Zhang, J.; Teng, F. *Sci. Rep.* **2015**, *5*, 9181.
(25) Li, Y.; Huang, H.; Wang, M.; Nie, W.; Huang, W.; Fang, G.; Carroll, D. L. *Sol. Energy Mater. Sol. Cells* **2012**, *98*, 273−276.
(26) Banerjee, A.; Shuai, Y.; Dixit, R.; Papautsky, I.; Klotzkin, D. *J. Lumin.* **2010**, *130*, 1095−1100.
(27) Gong, X.; Tong, M. H.; Xia, Y. J.; Cai, W. Z.; Moon, J. S.; Cao, Y.; Yu, G.; Shieh, C. L.; Nilsson, B.; Heeger, A. J. *Science* **2009**, *325*, 1665−1667.
(28) Jansen-van Vuuren, R. D.; Armin, A.; Pandey, A. K.; Burn, P. L.; Meredith, P. *Adv. Mater.* **2016**, *28*, 4766−4802.

DOI: 10.1021/acs.nanolett.6b05418
Nano Lett. 2017, 17, 1995−2002